ELSEVIER

Journal of Molecular Catalysis A: Chemical 146 (1999) 65–76

JOURNAL OF MOLECULAR CATALYSIS A: CHEMICAL

www.elsevier.com/locate/molcata

A new aspect of catalysis at designed surfaces: the role of gas phase molecules in surface catalytic reactions

Aritomo Yamaguchi, Kiyotaka Asakura, Yasuhiro Iwasawa *

Department of Chemistry, Graduate School of Science, The University of Tokyo, Hongo, Bunkyo-ku, Tokyo 113-0033, Japan

Received in revised form 28 December 1998

Abstract

This paper attempts to extend our previous studies on the chemical design and characterization of attached metal atoms at surfaces of a Nb/SiO_2 catalysts prepared by using a suitable metal-complex precursor and the elucidation of catalytic reaction mechanisms in a molecular scale. The paper also reports a new aspect of catalysis on a Co/Al_2O_3 catalyst which includes surface catalytic reactions assisted by gas phase molecules undetectable at the surface. On the basis of this concept, one may design new catalytic systems where the reaction intermediates, stable and unreactive in vacuum, can be activated or controlled by gas phase molecules in situ under catalytic reaction conditions.

Keywords: Catalytic reaction mechanisms; Design of active structures; Characterization by EXAFS and FT-IR; Nb/SiO_2; Co/Al_2O_3

1. Introduction

New and distinct materials and chemistry prepared stepwise in a controllable manner by using organic and inorganic metal complexes and clusters as precursors provide an opportunity for the development of efficient catalytic molecularly-organized surfaces en route to the ultimate catalyst technologies in the microscopic (atomic/molecular), mesoscopic, and macroscopic (mean-field) regions [1–6]. The notable superiority of this kind of catalytic systems is in single-site reactions, high selectivity, generality or wide applications, and tunability, which may be advantages of homogeneous catalysts. Homogeneous catalysts may be readily heterogenized so that the advantages of homogeneous catalysts on the one hand, their high specificity and tunability, and heterogeneous catalysts on the other, their built-in ease of separation of product from reactant, durability, stability and easy handling may be jointly harnessed in a synergistic mode at the surface. Synergistic phenomena at surfaces may be expected in a different manner from those in solutions because two different single-site structures can be organized at different places of a surface.

The longer term challenge to surface chemistry of oxide-supported metal catalysts is to address important issues in activity and selectiv-

* Corresponding author. Fax: +81-3-5800-6892; E-mail: iwasawa@chem.s.u-tokyo.ac.jp

1381-1169/99/$ - see front matter
PII: S1381-1169(99)00080-1

ity in catalytic reactions, in particular the principles of tuning of metal reactivity and activating reaction intermediates at oxide surfaces. In the development of new catalysts, new chemical concepts regarding structure or composition are conceived. The requirements and design of definite ensemble sizes represent important but as yet few addressed challenge to the field. The role of gas phase molecules in surface catalytic reactions remained to be solved to understand catalytic phenomena at surfaces under reaction conditions [7]. Recently molecular-level catalyst preparation has become realistic on the basis of modern physical techniques and accumulated knowledge of oxide surfaces, and a clear example of the surface catalytic reaction through strongly adsorbed intermediates assisted by weakly adsorbed molecules present only in the presence of the gas phase molecules has been uncovered on a designed Nb/SiO_2 catalyst [1,9,10].

The use of molecularly-designed catalysts seems to be prerequisite to examining the mechanism and concept of catalysis. There are several approaches to chemical design of active metal sites and ensembles on oxide surfaces by metal–organic and –inorganic complexes and clusters as shown in Table 1. It has been demonstrated that stable and active structures at catalyst surfaces can be prepared by reaction and strong interaction of inorganic and organic metal-complex precursors with oxides such as SiO_2, Al_2O_3, TiO_2, MgO, La_2O_3, zeolites, etc. In the catalysts obtained by this method (Category 1) metal atoms are attached to oxide surfaces via metal–oxygen bonding at metal–oxide interfaces. The attached metal atoms are often highly dispersed as monomers or distributed forming ensemble structures such as dimers and clusters by direct and oxygen-bonded metal–metal bondings depending on the oxidation state of attached metals, the acidity/basicity of oxide surfaces, the distribution of hydroxyl groups at oxide surfaces, etc.; e.g., Mo monomer/SiO_2 or Al_2O_3 [8], Nb monomer/SiO_2 or TiO_2 [9,10], chiral Rh monomer/SiO_2 [11], titanocene/MCM-41 [12], $V(acac)_3$–$Al(C_2H_5)Cl/SiO_2$ [13], Mo dimer/SiO_2 or Al_2O_3 [2,4,14,15], Nb dimer/SiO_2 [16], Rh dimer/SiO_2 [17,18], Ru_6C cluster/La_2O_3 or MgO [19,20], Nb_2O_5 monolayer/SiO_2 [1], ZrO_2 monolayer/ZSM-5 [21], etc. [1–6,8]. Active intermediates can be synthesized at oxide surfaces via attaching a metal complex with appropriate ligands to oxide surfaces, and subsequently chemical transformation of the ligands of the attached complex to reactive intermediate species (Category 2). A successful example of this method for surface design is Rh dimer/SiO_2 [17], in which an acyl ligand in a Rh dimer is produced by ligand-reactions among methyl, μ-methylene and carbonyl groups in situ at the SiO_2 surface. The obtained Rh dimer-acyl species attached on SiO_2 was active for ethene hydroformylation with a high selectivity of 88.9% under mild reaction conditions at a reduced pressure and 413 K, in contrast to only 5.6% with a conventional Rh/SiO_2 catalyst. Precursor complexes may be supported

Table 1
Typical approaches to chemical design of active metal sites and ensembles on oxide surfaces by metal–organic and –inorganic complexes and clusters

1	Selective reactions of complexes and clusters with surface OH groups: (a) Ligand–OH reactions, (b) Redox reactions, (c) Acid–base reactions
2	Surface synthesis and surface transformation
3	Electrostatic or electronic interaction at interface
4	Ship-in-a bottle synthesis
5	Epitaxial growth of active structures
6	Promoters (on, inside, near and far)
7	Selective element-exchange at cation and anion sites
8	Others (molecular imprinting, etc.)

on oxide surfaces by electrostatic interaction at interfaces (Category 3). An example is $Au(PPh_3)NO_3$ on $Fe(OH)_3^*$ or $Ti(OH)_4^*$, where the asterisk denotes as-precipitated wet metal hydroxides. The obtained $Au(PPh_3)_3NO_3$/as-precipitated hydroxides treated by temperature-programmed calcination were converted to tremendously active Au catalysts for low temperature CO oxidation [22–25]. It has been reported that ZrO_2 monolayers can be formed at the external surface of ZSM-5 by using $Zr(OC_2H_5)_4$ as a precursor. The ZrO_2 monolayer/ZSM-5 catalyst with Zr–Zr = 0.369 nm and Zr–O = 0.206 nm showed a high activity for methanol conversion to isopentane with a selectivity of 88.9% [21]. It seems that active tetragonal $ZrO_2(111)$ plane epitaxially grew on a ZSM-5(001) surface (Category 5). It is known that promoters placed on metal surfaces or close to metal particles can dramatically change catalytic performance of the metal (Category 6). A new approach to promoter effect has been reported with Ru_6C/La_2O_3 or MgO catalysts which were prepared using $[Ru_6C(CO)_{16}Me]^-$ with μ_6-carbide (interstitial carbido carbon) inside an octahedral Ru_6 framework as a precursor. The attached Ru_6C clusters exhibited the specific catalysis for CO conversion to oxygenated compounds such as methanol, dimethyl ether and formaldehyde, whereas conventional impregnated Ru catalysts mainly produced methane and hydrocarbons. The interstitial carbido carbon plays a decisive role in the control of selectivity to oxygenates in CO/H_2 conditions, where the interstitial carbon as central spring makes the cluster framework flexible to expand and shrink depending on the CO pressure and stabilizes the cluster framework under the reaction conditions [19,20]. Metal ions may be supported at oxide surfaces by replacing the cation sites of the oxide top layer (Category 7). An example is $[PtMo_6]/MgO$ which is prepared using $[PtMo_6O_{24}]^{8-}$ as a precursor. It has been demonstrated that Pt cations are located at the top layer substituting Mg cations of the MgO surface, showing Pt–O = 0.202 nm, Pt–Mg = 0.302 nm and Pt–O = 0.360 nm. The $[PtMo_6]/MgO$ catalyst was active for the dehydrogenation of propane, butane and isobutane to the corresponding alkenes without significant deactivation [26,27].

The present study reports the role of gas phase molecules in surface catalytic reactions as a new aspect of catalysis, using designed catalysts, Nb/SiO_2 and Co/Al_2O_3 with definite, active structures which are prepared by taking advantage of selective reactions of Nb and Co precursor complexes with surface OH groups of SiO_2 and Al_2O_3, respectively, in a key step for the catalyst preparation. The present preparations are regarded as a combination of the categories 1 and 2 in Table 1. The phenomena found on the designed catalysts were not clearly observed on traditional Nb/SiO_2 and Co/Al_2O_3 catalysts with heterogeneous surface structures prepared by a conventional impregnation method.

2. Experimental

2.1. Catalyst preparation

The attached Nb monomer catalyst (**3**) in Fig. 1 was prepared via the surface complex (**1**) which was obtained by reaction between $Nb(\eta^3\text{-}C_3H_5)_4$ and surface OH groups of SiO_2 at 233–273 K, followed by treatments with H_2 and O_2 [9,10]. SiO_2(Aerosil 200) was pretreated at 673 K in situ before use as a support for $Nb(\eta^3\text{-}C_3H_5)_4$. The surface complex (**1**), which was characterized by FT-IR, ESR and EXAFS, was the first to be highly active for propene metathesis [28]. The complex (**1**) was successively reduced with H_2 and oxidized with O_2 at 673 K to obtain the Nb^{5+} state (**3**). The Nb-carbide catalyst (**2**), which was characterized by O_2 titration and extended X-ray absorption fine structure (EXAFS), was found to be active for selective conversion of CO/H_2 to C_2–C_4 hydrocarbons in the Fischer–Tropsch synthesis [29]. The Nb^{5+} state in the catalyst (**3**) was

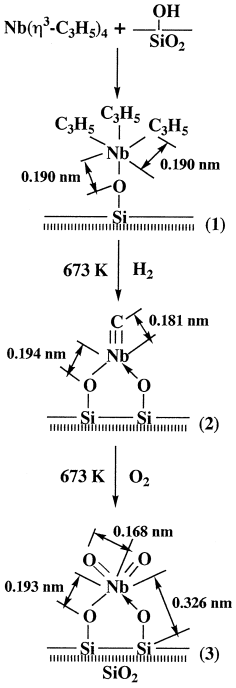

Fig. 1. Preparation steps for Nb/SiO_2.

confirmed by the XPS Nb 3d binding energies. The X-ray absorption near-edge structure (XANES) spectrum and diffuse reflectance Uv/Vis spectrum indicated a four-coordinated structure. The Nb–O, Nb=O and Nb–Si interatomic distances in the catalyst (**3**) were determined to be 0.193, 0.168 and 0.326 nm, respectively, by EXAFS. No Nb–Nb bonding was observed by EXAFS, demonstrating that the Nb^{5+} ions in the catalyst (**3**) are distributed as monomers [10]. The arrows in bonding scheme of Fig. 1 (species **2** and **3**) cannot be specified as a definite kind of bonding feature unlike the others; a candidate may be μ-oxo coordination from the surface.

A Co/Al_2O_3 catalyst was prepared in a similar manner to that reported in the literature [30–33]. $Co_2(CO)_8$ was attached on Al_2O_3 (Degussa Alon C) by a chemical vapor deposition method. Al_2O_3 was pretreated for 2 h at 573 K before use as a support for $Co_2(CO)_8$. Supporting $Co_2(CO)_8$ on the pretreated Al_2O_3 led to the formation of $Co_4(CO)_{12}$ (**4**) as shown in Fig. 2, with the release of one carbonyl ligand per Co atom. The $\sigma \rightarrow \sigma^*$ band of $Co_2(CO)_8$ related to the Co–Co bonding disappeared and was replaced by a new absorption peak at 413 nm with appearance of peaks at 270 and 595 nm, which were similar to the spectrum of the Al_2O_3-supported $Co_4(CO)_{12}$ cluster. The average Co–C bond distance was observed at 0.197 nm, which is comparable to that in a Co-tetramer rather than a Co-dimer. The species (**4**) with a Co–Co bond distance of 0.254 nm larger than 0.249 nm for C_{3v}–$Co_4(CO)_8$ was very sensitive to O_2 to be oxidized to a new species $[Co–O]_4/Al_2O_3$ (**5**), accompanied with disappearance of the direct Co–Co bond and appearance of a new Co–O bond at 0.205 nm which is

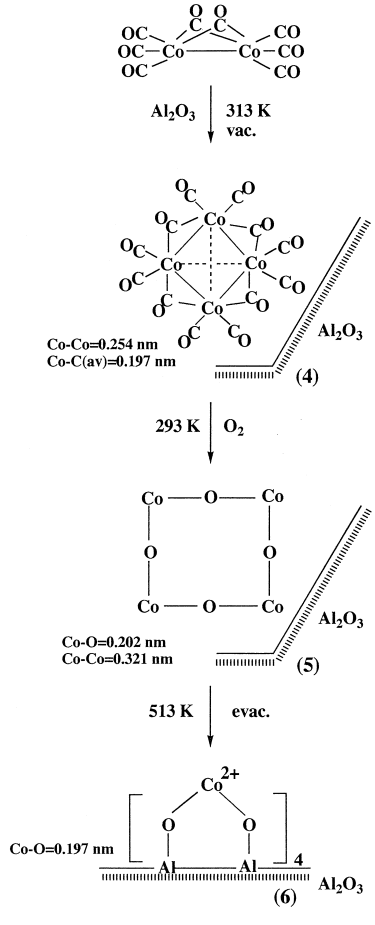

Fig. 2. Preparation steps for Co/Al_2O_3.

shorter than the Co–O bond in CoO crystal (0.2133 nm). The species (**5**) has not fully been characterized, but the Co atoms are suggested to be situated in a bivalent state with trigonally distorted tetrahedral symmetry by diffuse reflectance Uv/Vis spectra [30,31]. On heating to 513 K under vacuum, species (**5**) reacted with surface OH groups of Al_2O_3, as indicated by the decrease in the intensity of the ν(OH) band centered at 3550 cm^{-1}, to form a Co^{2+}/Al_2O_3 catalyst (**6**) accompanied with the formation of H_2O. The diffuse reflectance Uv/Vis spectrum of the catalyst (**6**) exhibited peaks at 657, 600 and 525 nm, indicating that the Co^{2+} ions are situated in a trigonally distorted T_d position. The bonding scheme of (**6**) in Fig. 2 is simply illustrated as a bivalent Co^{2+} structure with two Co–O bonds at 0.197 nm characterized by EXAFS. The T_d symmetry may be consistent with the formation of Co-dinitrosyls ($Co(NO)_2$) by coordination of two NO molecules as discussed hereinafter.

2.2. Catalytic reactions

Catalytic NO–CO reactions were carried out in a closed circulating system (dead volume: 205 ml) equipped with a gas chromatograph (Shimadzu GC-8A). A 2 m column of 5A Molecular Sieve and a 2 m column of Unibeads C were used for analyses of N_2, NO and CO, and N_2O and CO_2, respectively. The reactions of NO alone were also carried out in the same system. The detail of procedure for the catalytic ethanol dehydrogenation on Nb/SiO_2 is reported in the literature [10].

2.3. FT-IR measurements

FT-IR spectra were measured in an IR cell with two CaF_2 windows which were combined in a closed circulating system, on a JEOL KIR 7000 spectrometer. The spectra were recorded as difference spectra with a 2 cm^{-1} resolution and about 50 s time acquisition by a double-beam method, where the spectra for a sample cell with a catalyst wafer were subtracted by the spectra for the gas phase in a reference cell without catalyst wafer which was also combined in the closed circulating system. Thus the spectra were measured in situ under the catalytic reactions and the NO adsorption processes.

3. Results and discussion

3.1. Surface catalytic reactions assisted by gas phase molecules

A simplified form of the usual mechanism for heterogeneous catalytic reactions is shown in Fig. 3(a), where the reaction intermediate (**X**) is transformed to the product (**P**) by surface unimolecular decomposition; that is, a stoichiometric reaction step proceeds without aid of other molecules. In contrast to the simple expectation of no special role of additional gas phase molecules in a catalytic mechanism, we have found evidence that the reaction intermediate of an important catalytic reaction can be profoundly influenced by the ambient gas [7]. In the catalytic dehydrogenation reaction of ethanol on the Nb monomer catalyst, the intermediate (**X**) was stable and did not decompose to a product (**P**) up to 600 K, whereas in the coexistence of another reactant molecule (**A′**) the in-

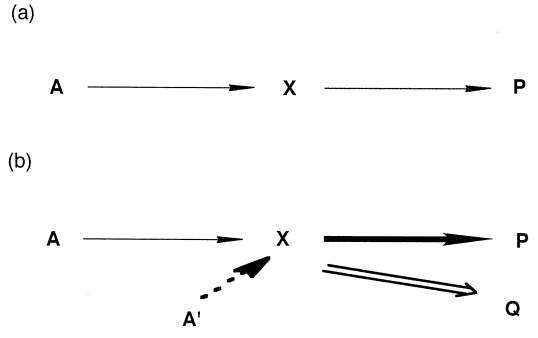

Fig. 3. Surface catalytic reactions assisted by gas phase molecules; (a) Surface catalytic reaction (**A** → **P**) via intermediate **X**; (b) Surface catalytic reaction (**A** → **P**) promoted by reactant molecule or coexisting molecule **A′**, where enhancement of the reaction rate for the formation of **P** or switchover of the reaction path from **P** formation to **Q** formation is caused by **A′**.

termediate (**X**) is activated to decompose to a different product (**Q**) even at low temperatures like 473 K, where the rate of the intermediate decomposition was enhanced and the reaction path was switched over as illustrated in Fig. 3(b) [7]. In this article two examples of surface catalytic reactions assisted by gas phase molecules are reported below, describing the previous finding of catalytic ethanol dehydrogenation on Nb monomers attached on SiO_2, promoted by weak coordination of additional ethanol that can be present only in the presence of gas phase ethanol, and presenting a new feature of catalytic NO–CO reaction at a Co/Al_2O_3 catalyst surface assisted by gas phase CO molecules undetectable at the surface.

3.2. Dehydrogenation of ethanol on Nb / SiO_2 and role of the gas phase ethanol molecules

The SiO_2-attached Nb catalyst (**3**) exhibited a high activity and selectivity for the dehydrogenation of ethanol. Acetaldehyde and hydrogen were stoichiometrically produced during the catalytic reaction. Ethanol dissociatively adsorbs on Nb to form ethoxyl ($C_2H_5O(a)$) and hydroxyl (OH(a)) as proved by FT-IR spectra. While $C_2H_5O(a)$ and OH(a) are only the adsorbed species under the catalytic reaction conditions, these adsorbed species are stable in vacuum. To gain insight into the reactivity of adsorbed ethanol, a temperature-programmed desorption (TPD) spectrum for the adsorbed species formed during the catalytic ethanol dehydrogenation reaction was measured. The TPD revealed that the reaction of adsorbed ethanol in vacuum was only possible at higher temperatures than 600 K, with a TPD peak at 700 K, and the products were ethene and water (dehydrated products). When the adsorbed species are exposed to the gas phase ethanol at 423–523 K, the dehydrogenation reaction to form acetaldehyde and hydrogen begins at these mild temperatures. Note that the behavior of adsorbed ethanol is entirely different in vacuum and in the presence of ambient ethanol [9,10]. The catalytic dehydrogenation reaction is assisted by the ambient ethanol, where the reaction path of adsorbed ethanol is switched from dehydration to dehydrogenation by the ambient ethanol. In other words, adsorbed ethanol prefers the dehydration to form ethene and water by the γ-hydrogen abstraction, while in the presence of the ambient ethanol the β-hydrogen abstraction from adsorbed ethanol to form acetaldehyde and hydrogen dominates as shown in Fig. 4 [7,10].

To examine how and why the surface ethanol reaction is assisted by the gas phase ethanol, the following experiments were conducted. Ethanol vapor was first admitted onto the Nb monomer catalyst (**3**) to form $C_2H_5O(a)$ and OH(a) at 373 K, followed by evacuation, and then the system was maintained at 523 K for 10 min, where neither hydrogen nor acetaldehyde were evolved because the adsorbed species were stable up to 600 K in vacuum. Then, various electron-donating compounds such as triethyl amine, pyridine, THF, diethyl ether, etc. were introduced to the surfaces preadsorbed with the same amount of ethanol, which led to a stoichiometric evolution of H_2 and CH_3CHO. As

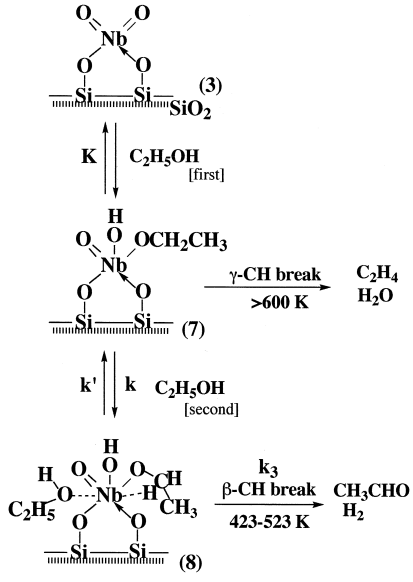

Fig. 4. Switchover of the reaction path by weak ethanol coordination.

the electron donating molecules have no extractable hydrogen, it is evident that both H_2 and CH_3CHO were produced from the preadsorbed ethanol by the assistance of the postdosed molecules. The logarithm of the initial rates of the CH_3CHO or H_2 formation from the preadsorbed ethanol was plotted against the donor number of the postadsorbed molecules which associatively adsorb on the Nb atom, where the donor number is defined as the logarithm of the equilibrium constant for the formation of electron donor–acceptor complexes between the nucleophilic molecules and $SbCl_5$ and regarded as the electron donor strength of the postadsorbed molecules. The linear relationship was observed, which indicates that the electron donor–acceptor interaction between the postadsorbed molecule and the coordinatively unsaturated Nb d^0 ion is a key issue for the dehydrogenation of the preadsorbed ethanol [10].

The postadsorbed ethanol (species **8** in Fig. 4) is weakly adsorbed on the Nb ethoxide monomer (species 7 in Fig. 4), which can be present only in the presence of gas phase ethanol, and it was kinetically characterized. Assuming the mechanism shown in Fig. 4, the rate constant k_3 and the equilibrium constant for weak adsorption of ethanol, k/k', were determined to be 1.5 mmol min^{-1} and 9.0×10^{-4} Pa^{-1}, respectively [10]. The weakly adsorbed ethanol is in equilibrium with the gas phase ethanol, and easily desorbs from the surface in vacuum.

The dehydrogenation mechanism reveals the switchover of the reaction path from dehydration (γ-CH bond break) to dehydrogenation (β-CH bond break) by whether or not ethanol molecules are present in the gas phase. In the presence of additional gas phase molecules, the catalytic reaction is able to proceed.

We have found another example of surface catalytic reactions assisted by gas phase molecules, where gas phase molecules participate as promoters in adsorption processes, but are undetectable at the catalyst surface, as described in Section 3.3.

3.3. Catalytic NO–CO reaction on Co/Al_2O_3 and role of the gas phase CO molecules

Slow N_2O formation from NO alone in a closed circulating system was observed above 350 K on the Co/Al_2O_3 catalyst (**6**). The N_2O formation at 463 K is still slow as shown in Fig. 5(a), and the amount of N_2O formed in the first 15 min of reaction was only ca. 2% of total Co quantity located at the catalyst surface. Hence, the observed rate of N_2O formation in the initial stage of reaction is not an apparent rate which has been affected by the oxygen atoms left on the catalyst surface. If CO alone was admitted to the fresh catalyst, no CO_2 was produced, indicating that there existed no reactive oxygen species on the fresh Co/Al_2O_3 catalyst (**6**).

The catalytic reaction of NO in the coexistence of CO to form N_2O and CO_2 by the equation $2NO + CO \rightarrow N_2O + CO_2$, proceeded rapidly compared to the reaction of NO alone as shown in Fig. 5(a) and (b). The initial rate of

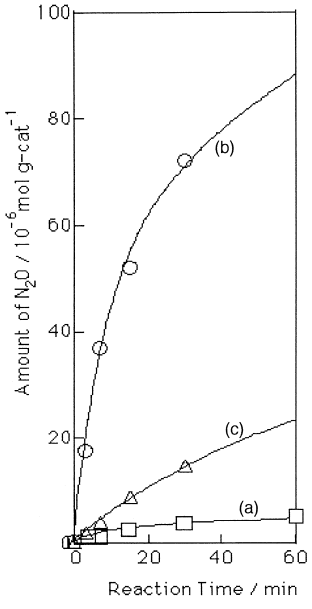

Fig. 5. NO reaction on the attached Co/Al_2O_3 catalyst (**6**) (a) and catalytic NO–CO reactions on the attached Co/Al_2O_3 catalyst (**6**) (b) and an impregnation Co/Al_2O_3 catalyst (c); Reaction temp.: 463 K; (a): NO = 1.3 kPa; (b) and (c): NO = 1.3 kPa + CO = 1.3 kPa; (a) and (b): Cat. = 0.50 g; Co loading = 2.2 wt.%; (c): Cat. = 0.50 g; Co loading = 3.0 wt.%.

the NO–CO reaction was 23 times larger than that for the NO reaction at 463 K. The activity of the Co/Al_2O_3 catalyst (**6**) was much higher than that of a conventional impregnation Co/Al_2O_3 catalyst as shown in Fig. 5. The products of the catalytic NO–CO reaction in the temperature range 353–463 K were N_2O and CO_2. In the more elevated temperatures N_2O was further converted to N_2, where N_2 and CO_2 were main products by the equations $2NO + CO \rightarrow N_2O + CO_2$ and $N_2O + CO \rightarrow N_2 + CO_2$. In this article the first reaction step, $2NO + CO \rightarrow N_2O + CO_2$, has been studied from the mechanistic interest.

The surface catalytic NO–CO reaction was monitored by IR spectroscopy and the gas phase products were analyzed by gas chromatography. Note that CO molecules which promote the surface NO conversion were volumetrically and spectroscopically undetectable as adsorbates on the Co/Al_2O_3 catalyst surface as shown in Fig. 6 [34]. Fig. 7 shows the IR spectra of adsorbed NO molecules under the ambient NO and in vacuum. The two peaks at 1831 and 1776 cm^{-1} are assigned to the dinitrosyl (geminal) NO species adsorbed on a Co atom ($Co(NO)_2$), as characterized by the isotope peaks at 1772 and 1701 cm^{-1} for $Co(^{15}NO)_2$ species and 1828 and 1735 cm^{-1} for $Co(^{14}NO)(^{15}NO)$ species. The intensity and relative intensity of the symmetric stretching peak at 1831 cm^{-1} and the antisymmetric stretching peak at 1776 cm^{-1} changed with exposure time and also by evacuation as shown in Fig. 7. The bond angle (θ) between the two NO ligands on a Co atom (angle: NO–Co–NO) has been demonstrated to be related to the ratio of the antisymmetric stretching peak intensity (I_{as}) to the symmetric stretching peak intensity (I_s) for the dinitrosyl groups by the equation, $I_{as}/I_s = \tan^2(\theta/2)$ (Fig. 8) [35]. The bond angles (θ) were calculated using this equation and plotted against exposure time in Fig. 9(a), where the θ was calculated by using the symmetric and antisymmetric stretching peaks after deconvolution. It is derived that the amount of adsorbed NO (n_{NO}) is proportional to $I_{as}/\sin^2(\theta/2)$ or $I_s/\cos^2(\theta/2)$, though n_{NO} is not absolute value for the amount of adsorbed NO. The calculated values of n_{NO} are plotted against time in Fig. 9(b). The change in n_{NO} coincided with the change in the amount of adsorbed NO determined gravimetrically in a separate experiment. Fig. 9(a) and (b) reveals

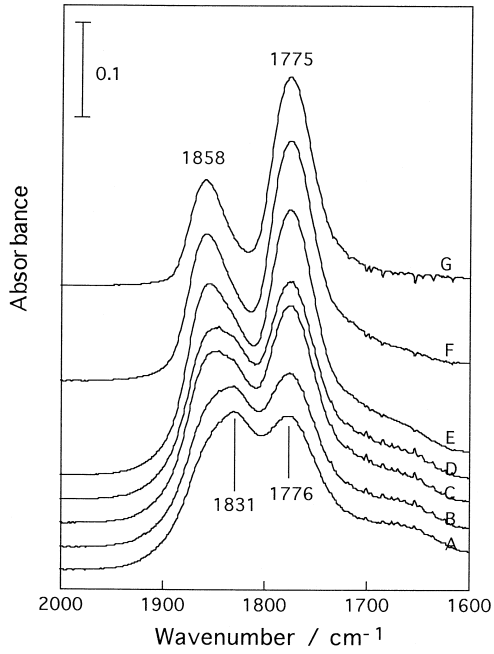

Fig. 7. FT-IR spectra for NO adsorbed on Co/Al_2O_3 (**6**) at 298 K; NO = 1.25 kPa; A–D: spectra at 2 min, 5 min, 30 min and 120 min after NO exposure, respectively; E–G: spectra after evacuation for 5 min, 30 min and 120 min after spectrum C, respectively.

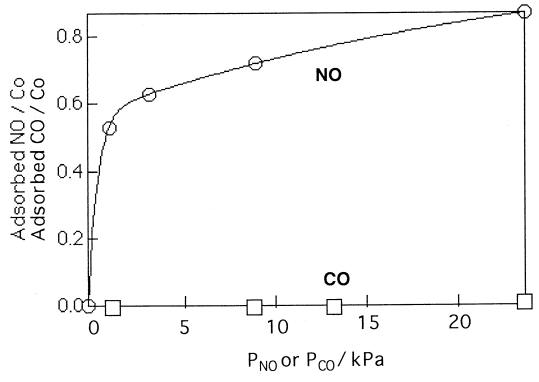

Fig. 6. Amounts of NO and CO adsorbed on Co/Al_2O_3 (**6**) at 298 K.

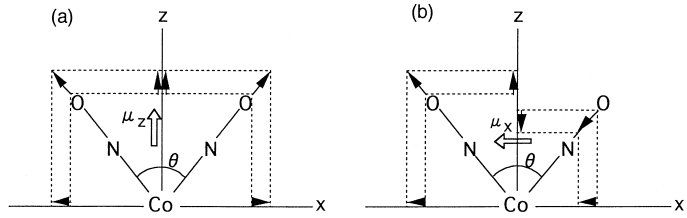

Fig. 8. Symmetric (a) and antisymmetric (b) stretching modes of the dinitrosyl on Co atom. μ_z and μ_x represent dynamic dipole moments induced by modes (a) and (b), respectively.

that there are two kinds of dinitrosyls (species A and species B); the dinitrosyl with a small bond angle (species A) is rapidly formed upon NO adsorption and easily desorbed by evacuation at room temperature, while the dinitrosyl with a large bond angle (species B) is slowly formed and not desorbed by evacuation at room temperature. We estimate the ratio of species A to species B to be 1: 1.9 at room temperature. As the bond angle θ of species B was 107° and the bond angle for a mixture of species A and species B at 120 min of Fig. 9 was 97°, the θ for species A at room temperature was estimated to be 80°.

Fig. 10 shows the effects of CO on the bond angle and amount of adsorbed NO at 323, 373, 423, 448 and 463 K. The amount of the dinitrosyls decreased with increasing temperature, while the bond angle θ increased with an increase of temperature. When CO was introduced to the system, the bond angle θ of the surface dinitrosyls increased. The degree of the angle expanding was different at temperatures and larger at higher temperatures, and at 323 K

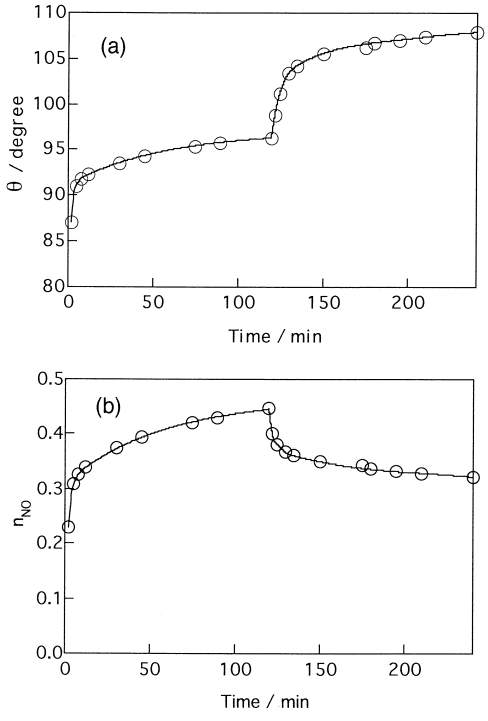

Fig. 9. Time profiles of the bond angle and amount of dinitrosyls on Co/Al_2O_3 (**6**) at 298 K; NO of 1.25 kPa was exposed at time zero and evacuated at 120 min.

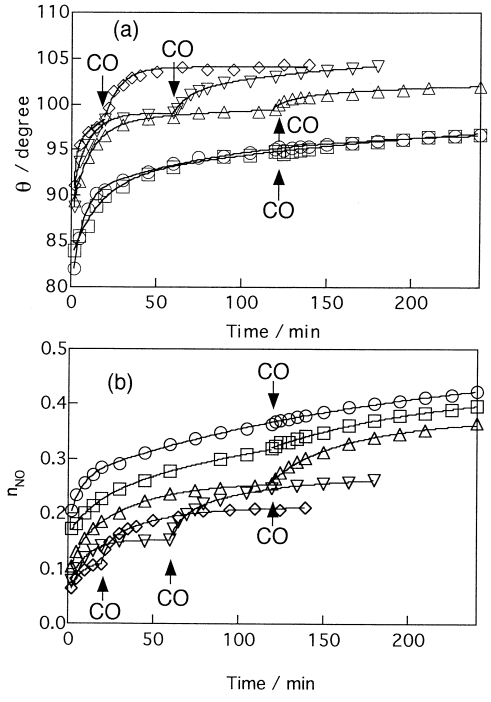

Fig. 10. Time profiles and CO effects of the bond angle (θ) and amounts of dinitrosyls on Co/Al_2O_3 (**6**); NO: 1.3 kPa; CO: 1.3 kPa; ○: 323 K; □: 373 K; △: 423 K; ▽: 448 K; ◇: 463 K.

almost no effect was observed. It was also found that the amount of the dinitrosyls increased by CO admission. Again, the degree of the increase was larger at higher temperatures. At 463 K, the amount of the dinitrosyls was increased by the presence of the gas phase CO about twice as compared to the amount in the case of NO alone. The enhancement of the NO adsorption by the gas phase CO was not observed at 323 K. Thus, the effects of the ambient CO were large at the temperatures where the catalytic NO–CO reactions proceeded significantly, whereas the bond angle and amount of the dinitrosyls did not change by the presence of CO at 323 K, where the catalytic NO–CO reaction was negligible.

The property of the Co^{2+} sites for adsorption is different from that of Mo sites prepared from $Mo(CO)_6$ where $Mo(NO)_2(CO)$ has been proposed [36]. As CO is not observed at the surface, the conformation change to the spacious dinitrosyls and the increase of the amount of adsorbed NO might be collision-induced events. The catalytic reaction rate (υ) was expressed by $\upsilon = k[NO]^{1.6}[CO]^{0.95}$ in the pressure range 0.26–4.0 kPa. The catalytic reaction rate is nearly proportional to CO pressure, which might also provide a picture of CO collision on the Co-dinitrosyl. However, N_2 and Ar showed no effect on the adsorbed NO species at 463 K, which would exclude a possibility of the θ extension and the n_{NO} increase by a physical collision energy. Other explanation is necessary for the θ extension and the n_{NO} increase; for example, the CO molecules may have a short resident time on the Co^{2+} sites to have interaction with the dinitrosyls, which depends on the surface temperature. As the amount of adsorbed CO is undetectable volumetrically and spectroscopically, the formation of the spacious dinitrosyl species must be irreversible and the backward change of a spacious conformation (107°) to a small conformation (80°) may be at least much slower than the impinging rate of CO. We do not know the exact reason for the observed events at present, but this phenomenon may involve a local structural change of the Co^{2+}–Al_2O_3 interface by CO impinging under the catalytic NO–CO reaction conditions.

4. Summary

The catalytic ethanol dehydrogenation proceeds through Nb ethoxide intermediates (**7**). However, the species (**7**) is stable and is not decomposed to CH_3CHO and H_2 at 423–523 K in vacuum. Instead, the species (**7**) is converted to C_2H_4 and H_2O at so high temperatures as 700 K. On the other hand, the unreactive Nb-ethoxide (**7**) is transformed to reactive Nb-ethoxide (**8**) under the catalytic reaction conditions, where weak ethanol coordination can be present on a vacant site of the species (**8**) and electronically activate the Nb ethoxide (**8**) to produce CH_3CHO and H_2. The dehydrogenation mechanism reveals the switchover of the reaction path from dehydration (γ-CH bond break) to dehydrogenation (β-CH bond break) of the intermediate (**X**) by whether or not ethanol molecules are present in the gas phase. The catalytic ethanol dehydrogenation reaction on the Nb/SiO_2 catalyst is able to proceed only in the presence of additional gas phase molecules (**A′**).

The enhancement of the rate of the intermediate decomposition and the switchover of the reaction path were also found in water–gas shift reactions on MgO, ZnO and Rh/CeO_2 [5,37–39]. These examples presented a new aspect of catalysis, namely, that surface catalytic reaction pathways are made accessible only under the ambient gas [7]. It has also been reported that the reactivity of the formate ions on Ni/SiO_2 catalyst was markedly increased by the presence of formic acid in the ambient gas compared to that at the same coverage under vacuum though the mechanism is not clear [40].

The catalytic NO–CO reaction on the Co/Al_2O_3 catalyst (**6**) proceeds through the dinitrosyls as reaction intermediates (**X**) which conformation and amount are affected by the

gas phase CO molecules. There is no CO molecules at the catalyst surface during the catalytic reactions. The reactivity of the dinitrosyls on the trigonally distorted tetrahedral Co^{2+} ions attached on Al_2O_3 is promoted 23 times by the gas phase CO molecules. In this reaction mechanism, impinging CO molecules (**A′**) are spectators at the catalyst surface, but they change the conformation and amount of the active species (**X**), and also behave as reactant. It is to be noted that molecules undetectable at surface can give profound effects on the surface structure of reaction sites and promote remarkably the reactivity of surface species.

The following examples may be categorized in a different class of surface catalytic/stoichiometric reactions assisted by gas phase molecules, where the phenomena involve strong adsorption of gas phase molecules. Au and Roberts observed that the surface oxygen transient generated during the dissociative chemisorption of the coadsorbed promoter molecules such as O_2, NO and N_2O on Mg(0001) was active for H-abstraction of NH_3, while chemisorbed oxygen overlayer was relatively unreactive [41]. Sasaki et al. found a remarkable enhancement of the NH_3 decomposition on Ru(001) by coexistence of CO which is not involved in the reaction [42,43]. Burke and Madix demonstrated that the introduction of CO onto the surface presaturated with hydrogen and ethene brought about the formation of ethane, a reaction which did not occur in the absence of CO [44]. Rodrigues et al. observed promotional effect of a small amount of added CO on the growth of filamentous carbon from a C_2H_4–H_2 mixture at 873 K on a Fe catalyst [45].

As described above, weakly adsorbed molecules or impinging molecules under catalytic reaction conditions play an important role in surface catalytic reactions even if the adsorption of ‘promoter’ is very weak or is undetectable [7]. Stable adsorbates are activated and the selectivity of the surface reaction is changed drastically under the ambient gas. Phenomenon described in this article may be extended to many catalytic systems. The concept of surface catalytic reactions assisted by weak or undetectable coordination may provide an approach to design new catalytic systems through activation or control of inactive and stable surface sites in situ under catalytic reaction conditions.

Acknowledgements

The authors thank Dr. M. Nelson, Mr. S. Takahara, and Ms. A. Kameyama for her data acquisitions and helpful discussion. A part of this work has been supported by CREST (Core Research for Evolutional Science and Technology) of the Japan Science and Technology (JST).

References

[1] Y. Iwasawa, Stud. Surf. Sci. Catal. 101 (1996) 21, Proc. 11th Int. Congr. Catal. Baltimore, Elsevier, Amsterdam.
[2] Y. Iwasawa, Adv. Catal. 35 (1987) 187.
[3] Y. Iwasawa, Catal. Today 18 (1993) 21.
[4] Y. Iwasawa (Ed.), Tailored Metal Catalysts, Reidel, Dordrecht, 1987.
[5] Y. Iwasawa, in: R.W. Joyner, R.A. van Santen (Eds.), Elementary Reaction Steps in Heterogeneous Catalysis, Vol. 398, NATO ASI Ser. C, 1993, p. 287.
[6] B.C. Gates, L. Guczi, H. Knözinger (Eds.), Metal Cluster in Catalysis, Elsevier, Amsterdam, 1986.
[7] Y. Iwasawa, Acc. Chem. Res. 30 (1997) 103.
[8] Yu.I. Yermakov, B.N. Kuznetsov, V.A. Zakharov, Catalysis by Supported Complexes, Elsevier, Amsterdam, 1981.
[9] M. Nishimura, K. Asakura, Y. Iwasawa, J. Chem. Soc. Chem. Commun. (1986) 1660.
[10] M. Nishimura, K. Asakura, Y. Iwasawa, Proc. 9th Int. Congr. Catal. Calgary 4 (1988) 1566.
[11] B. Pugin, F. Spindler, M. Müller, EP 496699-A1(1991); EP 496700-A1(1991).
[12] J.M. Thomas, J. Mol. Catal. A: Chemical 115 (1997) 371.
[13] Union Carbide, US Patent 5342907A(1994).
[14] S. Sato, Y. Iwasawa, H. Kuroda, Chem. Lett., (1982) 1101.
[15] Y. Iwasawa, K. Asakura, H. Ishii, H. Kuroda, Z. Phys. Chem. N. F. 144 (1985) 105.
[16] N. Ichikuni, Y. Iwasawa, Proc. 10th Int. Congr. Catal. Budapest, 1993, p. 477.
[17] K. Asakura, K.K. Bando, Y. Iwasawa, H. Arakawa, K. Isobe, J. Am. Chem. Soc. 112 (1990) 9096.
[18] K.K. Bando, K. Asakura, H. Arakawa, K. Isobe, Y. Iwasawa, J. Phys. Chem. 100 (1996) 13636.
[19] Y. Izumi, T. Chihara, H. Yamazaki, Y. Iwasawa, J. Phys. Chem. 98 (1994) 594.

[20] Y. Izumi, Y. Iwasawa, Chemtech 24 (1994) 20.
[21] K. Asakura, M. Aoki, Y. Iwasawa, Catal. Lett. 1 (1988) 395.
[22] Y. Yuan, K. Asakura, H. Wan, K. Tsai, Y. Iwasawa, Chem. Lett. (1996) 755.
[23] Y. Yuan, A.P. Kozlova, K. Asakura, H. Wan, K. Tsai, Y. Iwasawa, J. Catal. 170 (1997) 191.
[24] A.P. Kozlova, S. Sugiyama, A.I. Kozlov, K. Asakura, Y. Iwasawa, J. Catal. 176 (1998) 426.
[25] Y. Yuan, K. Asakura, A.P. Kozlova, H. Wan, K. Tsai, Y. Iwasawa, Catal. Today 44 (1998) 333.
[26] D.I. Kondarides, K. Tomishige, Y. Nagasawa, Y. Iwasawa, in: G. Poncelet et al. (Eds.), Preparation of Catalysts VI, Elsevier, Amsterdam, 1995, p. 141.
[27] D.I. Kondarides, K. Tomishige, Y. Nagasawa, U. Lee, Y. Iwasawa, J. Mol. Catal. A: Chemical 111 (1996) 145.
[28] M. Nishimura, K. Asakura, Y. Iwasawa, Chem. Lett. (1986) 1457.
[29] M. Nishimura, K. Asakura, Y. Iwasawa, Chem. Lett. (1987) 573.
[30] M. Yamada, Y. Iwasawa, Nikkashi (1984) 1042.
[31] Y. Iwasawa, M. Yamada, Y. Sato, H. Kuroda, J. Mol. Catal. 23 (1984) 95.
[32] Y. Iwasawa, Supported catalysts from chemical vapor deposition and related techniques, in: G. Ertl, H. Knözinger, J. Weitkamp (Eds.), Handbook of Heterogeneous Catalysis, Vol. 2, Wiley-VCH, New York, 1997, p. 853.
[33] K. Asakura, Y. Iwasawa, J. Phys. Chem. 93 (1989) 4213.
[34] Y. Iwasawa, Abstract of 7th Japan–China–USA Symposium on Catalysis, Tokyo, 1995, p. 49.
[35] P.S. Braterman, Metal Carbonyl Spectra, Academic Press, New York, 1975, p. 43.
[36] J. Goldwasser, S.M. Fang, M. Houalla, W.K. Hall, J. Catal. 115 (1989) 34.
[37] T. Shido, K. Asakura, Y. Iwasawa, J. Catal. 122 (1990) 55.
[38] T. Shido, Y. Iwasawa, J. Catal. 129 (1991) 343.
[39] T. Shido, Y. Iwasawa, J. Catal. 140 (1993) 575.
[40] K. Takahashi, E. Miyamoto, K. Shoji, K. Tamaru, Catal. Lett. 1 (1988) 213.
[41] C.-T. Au, M.W. Roberts, J. Chem. Soc., Faraday Trans. 1 83 (1987) 2047.
[42] T. Sasaki, T. Aruga, H. Kuroda, Y. Iwasawa, Surf. Sci. Lett. 224 (1989) L969.
[43] T. Sasaki, T. Aruga, H. Kuroda, Y. Iwasawa, Surf. Sci. 240 (1990) 223.
[44] M.L. Burke, R.J. Madix, J. Am. Chem. Soc. 113 (1991) 3675.
[45] N.M. Rodriguez, M.S. Kim, R.T.K. Baker, J. Catal. 144 (1993) 93.